CW or Pulsed laser – That is the Question: Comparative Steady-state Photocrystallographic Analysis of Metal Nitrosyl Linkage Isomers

Asma Hasil, Krzysztof Konieczny, Artem Mikhailov, Sébastien Pillet, Dominik Schaniel

CW or Pulsed laser — That is the Question: Comparative Steady-state Photocrystallographic Analysis of Metal Nitrosyl Linkage Isomers

Dr. Asma Hasil[*], *Dr. Krzysztof A. Konieczny*, *Dr. Artem Mikhailov*, *Dr. Sébastien Pillet and Prof. Dr. Dominik Schaniel*

Université de Lorraine, CNRS, CRM2, F-54000 Nancy (France)
E-mail: asma.hasil@univ-lorraine.fr, dominik.schaniel@univ-lorraine.fr

Abstract

The investigation of photo-induced effects is profoundly influenced by the characteristics of photo-excitation sources. In this study, we present a comprehensive analysis of the structures of two photoinduced linkage isomers (PLI) in a ruthenium nitrosyl complex trans-$[Ru(py)_4F(NO)](ClO_4)_2$, following irradiation with both pulsed and continuous wave (CW) light sources under low temperature conditions. The X-ray (photo)diffraction analysis shows that the resulting PLI generated from the two types of irradiation sources, an isonitrosyl configuration of the nitrosyl ligand in the so-called metastable state MS1, and a side-on configuration of the nitrosyl ligand in the metastable state MS2, are identical. In-situ optical absorption spectroscopy was employed during CW and pulsed irradiation, enabling the monitoring of the population process of these PLI. The results obtained from the infrared spectroscopic analysis after pulsed irradiation give insight into the population mechanism illustrating that the generation of the isonitrosyl MS1 occurs through a two-step process, *via* the second PLI, the side-on configuration MS2.

Introduction

In most general terms, photocrystallography [1–4] deals with the study of the structure and properties of materials that can be modified by light. From the study of the light-induced processes in photosynthesis [5] to the investigation of solid-to-liquid phase transitions in semiconductors induced by femtosecond laser pulses, [6] X-ray diffraction has been used to help unravel the structural modifications at the heart of the physical, chemical and biological processes. This vast range of studied phenomena requires the use of a large diversity of irradiation sources, from lamps simulating the solar spectrum to high-power pulsed lasers with varying pulse duration. The type of the used photoirradiation source might also influence the light-induced effects that can be observed, e.g. in the cases where the photoinduced dynamics is triggered only above a certain threshold such as photoinduced phase transitions (PIPT) or when cooperative phenomena play a crucial role [7–9]. It is therefore relevant to study the influence of the nature of the photoexcitation source on the light-induced effect. We can distinguish between continuous wave (CW) sources such as CW lasers or lamps and light-emitting diodes (LED) and pulsed irradiation sources such as nano- or femtosecond pulsed lasers. The former are used in low-power applications, such as molecular switching [10,11] while the latter may provide very high peak powers and hence lead to the observation of non-linear phenomena but sometimes also induce significant material damage. In order to overcome the issue of photoinduced damage and at the same time maximize photoconversion, Hatcher and coworkers [12] recently demonstrated the utility of using pulsed LED light with durations of 0.4 s or longer on the example of a Pd-NO_2 linkage isomer. Nevertheless, pulsed excitation sources are a must if one wants to study ultrafast structural dynamics [3].

In the field of photoinduced linkage isomers (PLI) mostly CW sources have been used for the photocrystallographic studies [13–19], since the PLI can be stabilized at low temperature and hence studied by steady-state X-ray diffraction (XRD). In order to investigate the structural dynamics during formation of PLI the use of pulsed excitation sources becomes necessary, and therefore the influence of the type of excitation source on the resulting PLI needs to be investigated. As a particular type of PLI, linkage isomers of the NO ligand are found in $\{MNO\}^6$ -type complexes, where M designs a transition metal and 6 is the number of metal d-electrons if NO^+ is considered to be the ligand (Enemark-Feltham notation [20]). In $\{MNO\}^6$ complexes two PLI can be generated from the linearly bound NO ligand (*l*-NO-κ*N*) in the ground state (GS) : the linear isonitrosyl *l*-NO-κ*O* (MS1) and the side-on bound NO-κ^2*N,O* (MS2) [21], which are also often referred to as metastable state 1 (MS1) and 2 (MS2), due to the fact that at low temperature their lifetime becomes very long (up to years). Within this large family of compounds, $[Ru(py)_4F(NO)](ClO_4)_2$ is a very interesting case, since the population of MS1 is almost 100% and the two linkage isomers configurations MS1 and MS2 exhibit a very high thermal stability, with lifetimes at room temperature of about 150 s and 18 ms, respectively [22]. It is a close relative of $[Ru(py)_4Cl(NO)](PF_6)_2$ which exhibits an equally high population of MS1 [23] and for which a number of theoretical studies are available with respect to the photoisomerization mechanism [24–26]. These studies clearly hint to a two-step mechanism from GS to MS2 and then to MS1. From the experimental point of view this two-step mechanism was investigated spectroscopically [22,27], where in the case of $[Ru(py)_4F(NO)](ClO_4)_2$ transient absorption spectroscopy after excitation by single nanosecond laser pulses revealed a temporal signature compatible with MS2 while infrared spectroscopy after repeated nanosecond pulsed laser excitation yielded the signature of MS1 [22].

In the present work linkage isomerism is studied in trans-$[Ru(py)_4F(NO)](ClO_4)_2$ (**I**) using both type of irradiation sources i.e., CW and pulsed light sources. **I** contains two independent $[Ru(py)_4F(NO)]^{2+}$ molecules in the unit cell, which exhibit different PLI properties, namely different populations of MS2 as mentioned in our previous article [22] and slightly different thermal stabilities of MS1 as investigated in more detail by photo-NMR [28]. In order to unambiguously link the MS1 and MS2 structures obtained from XRD to the spectral signatures obtained from infrared and absorption spectroscopy we therefore performed a comparative study of these PLI in (**I**) after pulsed and CW excitation on our laboratory XRD setup allowing for in-situ optical absorption measurements [29] in parallel to the single-crystal XRD. The results are discussed with respect to the characteristics of the used excitation source and compared to those from our previously reported photocrystallographic study using CW sources for PLI generation [22].

Experimental details

CW vs pulsed excitation

The two types of photo-irradiation sources have some key differences in terms of their characteristics and applications. A CW laser produces a continuous beam of laser light and can be used to provide the necessary excitation energy (wavelength) with constant intensity over a given irradiation time. Alternatively, a pulsed laser source, emits a series of short pulses of laser light characterized by the pulse duration, repetition rate and energy density, to provide the required excitation energy in short but intense pulses to the sample (see Figure 1). For our purpose, it is important to know the number of photons (eq. 1) impinging on the measured crystal with surface $A_{crystal}$

$$n_{photons\ on\ crystal\ surface} = \frac{e_{laser} A_{crystal}}{hc} \quad (1)$$

where e_{laser} is the energy density, $A_{crystal}$ is the area of the crystal exposed to light, h the Planck constant 6.62607015×10^{-34} Js, and the speed of light c = 299792458 ms^{-1}. This number can then be compared to the number of molecules present in the corresponding crystal volume to estimate the photoswitching efficiency using eq. (2). For more details concerning these calculations see supplementary information.

$$Z_{molecules} = \frac{V_{crystal} Z_{unit\ cell}}{V_{unit\ cell}} \quad (2)$$

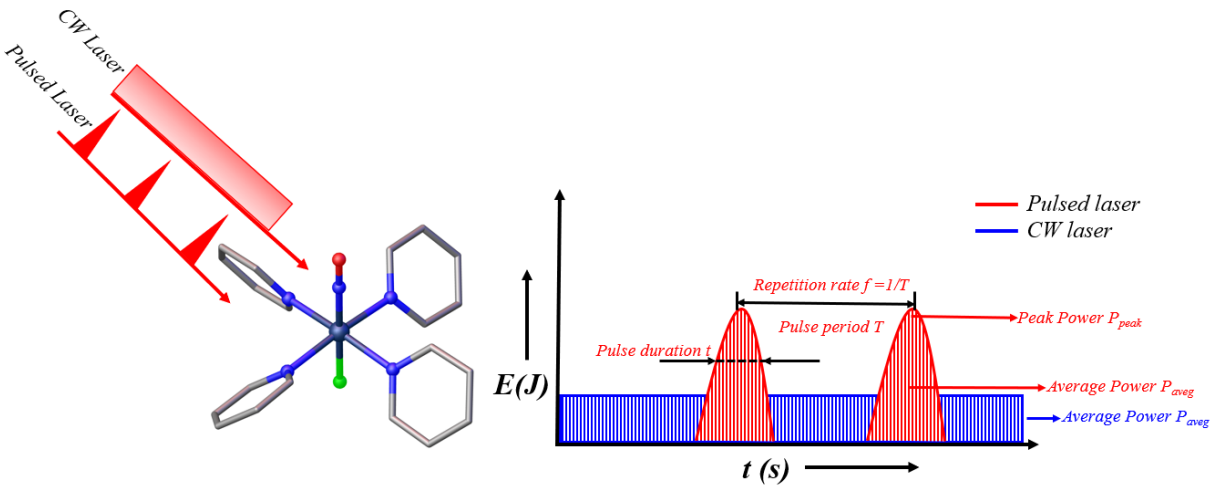

Figure 1: Structure of $\{MNO\}^6$ type $[Ru(Py)_4(NO)F]^{2+}$ complex (left panel). Comparison of the temporal shape of CW laser and pulsed laser output (right panel).

The following CW irradiation sources were used for the XRD and infrared spectroscopic experiments: A Coherent OBIS 422 nm CW laser was used for the generation of MS1 and a Thorlabs 940 nm LED for the generation of MS2. For the pulsed excitation two different Nd-YAG pumped optical parametric oscillators (OPO) were used for XRD and infrared spectroscopy: an EKSPLA NT340 (**A**) series nanosecond pulsed laser for XRD and a Continuum Surelite II (**B**) nanosecond pulsed laser for the infrared spectroscopic experiments (Table 1). Both lasers were used at a repetition rate of 10 Hz (except for the shot-by-shot experiments) and exhibit a pulse length of 3-5 ns. The pulse energy density was adjusted by λ/2 waveplates and polarizers.

Table 1: The CW and pulsed photo-irradiation sources used during the experiments in the present study.

Photoirradiation source			Application	
Type	Model	Specifications	XRD/in-situ UV-Vis	IR
CW	Coherent OBIS 422 Laser	λ = 422 nm (monochromatic)	MS1 generation	MS1 generation
	Thorlabs M940L3 LED	λ = 940 nm (center wavelength)	Transfer MS1 to MS2	Transfer MS1 to MS2
Pulsed	EKSPLA NT340 (**A**)	λ tuneable from 192-2600 nm, maximum repetition rate 20 Hz, pulse width 3-5 ns	MS1 generation λ = 422 nm, (monochromatic) Transfer MS1 to MS2 λ = 940 nm, (monochromatic)	-
	Nd-YAG Continuum Surelite II (**B**)	λ tuneable from 410-2500 nm, maximum repetition rate 20 Hz, pulse width 3-5 ns	-	MS1 generation λ = 422 nm, (monochromatic) Transfer MS1 to MS2 λ = 940 nm, (monochromatic)

X-ray diffraction with in-situ UV/Vis absorption spectroscopy

Single crystal data collection was performed at 100 K (N_2 blower) in GS and PLI states using the STOE Stadivari diffractometer in 4-circle Eulerian cradle geometry, a RebirX 540S CEGITEK hybrid pixel area detector (HPAD) and a microfocus Mo Kα source (λ = 0.71073 Å). Unit cell determination and data reduction was performed using the *X-AREA* program suite [30]. The corresponding structure was solved in the space group *P*-1 with the *SHELXT* [31] structure solution program using intrinsic phasing and refined with the *SHELXL* [32] refinement package using least-squares minimization embedded in *Olex2-1.5-alpha* suite [33]. All non-H atoms were refined anisotropically, except of the MS1B structure collected after pulsed irradiation, where both MS1 and GS components of the NO ligands were refined isotropically. A riding model [34] was used for hydrogen atoms attached to pyridine. Corresponding data collection and refinement parameters are given in Table 2. The refinements are further detailed in the supplementary information section S2.2. For the photogeneration of MS1 and MS2, two setups were used: one for CW excitation, and one for pulsed laser excitation.

For the CW irradiation, appropriate CW lasers or LEDs (see table 1) were mounted on the optical table as indicated in the scheme (Figure 2). For pulsed irradiation, pulsed laser **A** (see table 1) is a peripheric device (outside diffractometer cabinet) and the beam was guided by a set of mirrors in the following order: M1'-M4' (peripheric mirrors), M1-M5 (cabinet mirrors). Afterward, the beam is focused onto the crystal by lens 1 (L1). The beam power can be adjusted directly from the laser interface. However, for convenience, *λ*/2 wave plate and polarizer P are mounted between M4 and L1 for precise power regulation. If additional beam diagnostic is necessary, a beam splitter BS (removable/ exchangeable with mirror 5, M5) guiding the laser beam to the photodiode connected to the oscilloscope can be mounted. Finally, the beam was aligned on the crystal sample position by using a 500 µm pinhole, and the maximum power at the sample position was determined. The set-up is shown in Figure 2.

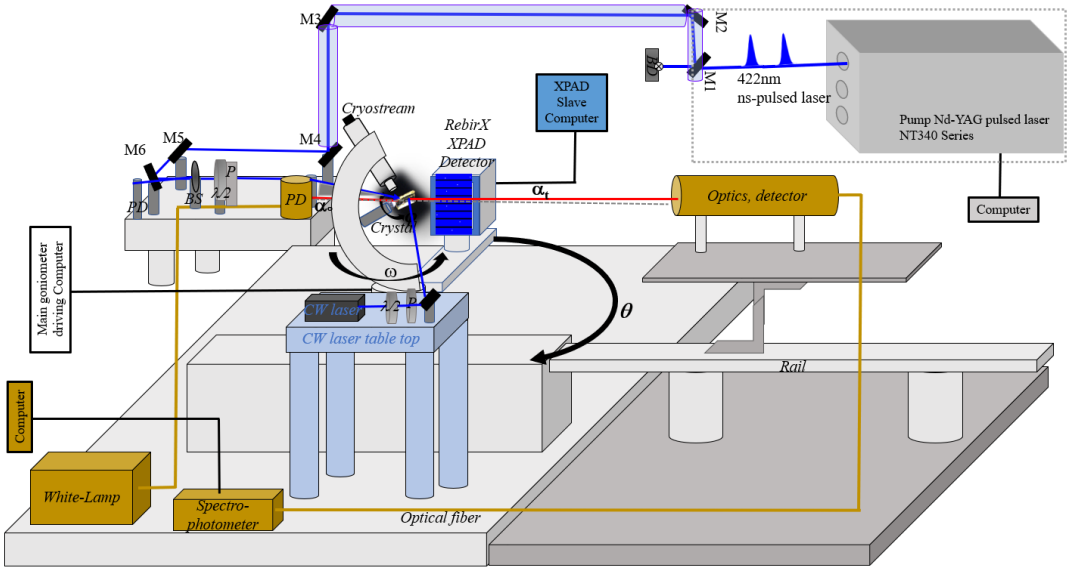

Figure 2: Schematic in-house setup for the photocrystallographic and optical absorption measurements of single crystals. The abbreviation used in the scheme: photodiode PD, beam splitter BS, beam dump BD, polarizer P and mirrors M.

If the PLI have different absorption spectra compared to the GS in the visible region, the progress of the conversion from GS to PLI can be monitored by using optical spectroscopy [35]. The characterization by optical absorption (OA) spectra of the single crystal will aid in revealing the differences/similarities in the CW and pulsed laser irradiation and will help to analyze the structure-property relationships. For recording the OA spectra, a white light lamp (100 W quartz tungsten halogen QTH) with Oriel 77501 housing was used and connected through an optic fiber (Ø 200 µm) connector to the lens tube and then guided by a series of lenses to focus the beam on the crystal sample, that is mounted on the goniometer head. For signal acquisition, a customized apochromatic photographic objective was used in combination with a beam expander, with adjustable distance, to obtain a spot size of few microns (25 – 250 µm) on the position of the crystal sample. The spectra were collected using an Ocean Optics spectrometer. More details on this setup for in-situ OA measurements on single crystals will be given in [29]. The experiment was conducted as follows. After photoexcitation by CW or pulsed laser, the OA spectra of the PLI were recorded. After each OA measurement, a photograph of the crystal was recorded using the centering camera of the diffractometer in order to monitor the photoinduced changes and possible damage on the surfaces. Finally, X-ray diffraction data are collected to determine the photoinduced structural changes.

Infrared spectroscopy

Infrared spectroscopy allows to identify the PLI due to their distinct vibrational properties, especially the position of the NO stretching vibration can serve as a fingerprint for GS, MS1 and MS2 in $\{MNO\}^6$ type compounds [36]. The IR spectra were collected before, during and after irradiation with CW or pulsed laser at 422 nm using a Nicolet 5700 FTIR, with a resolution of 2 cm^{-1}. Temperature was controlled by a cryostat (Optistat V01). Samples were prepared as KBr pellets, using a well-defined amount of **I** and KBr in order to determine precisely the number of molecules present in the pellet. The pulsed laser source **B** was used in this experiment (see table 1) while CW laser is the same as used in OA and photocrystallography experiments.

Results

Figure 3 illustrates the GS structure and packing of **I**. The unit cell contains two independent $[Ru(py)_4F(NO)]^{2+}$ molecules with central Ru1 and Ru2 atoms (Fig.3 (a)); with bond distances Ru1–N1 1.768(1) Å and Ru2–N6 1.760(1) Å, and Ru1–N1–O1 179.0(1)° and Ru2–N6–O2 177.3(1)° bond angles in molecule one and two, respectively (see Tables 1, 2 and S1-S3 for full list of cell parameters, distances and angles).

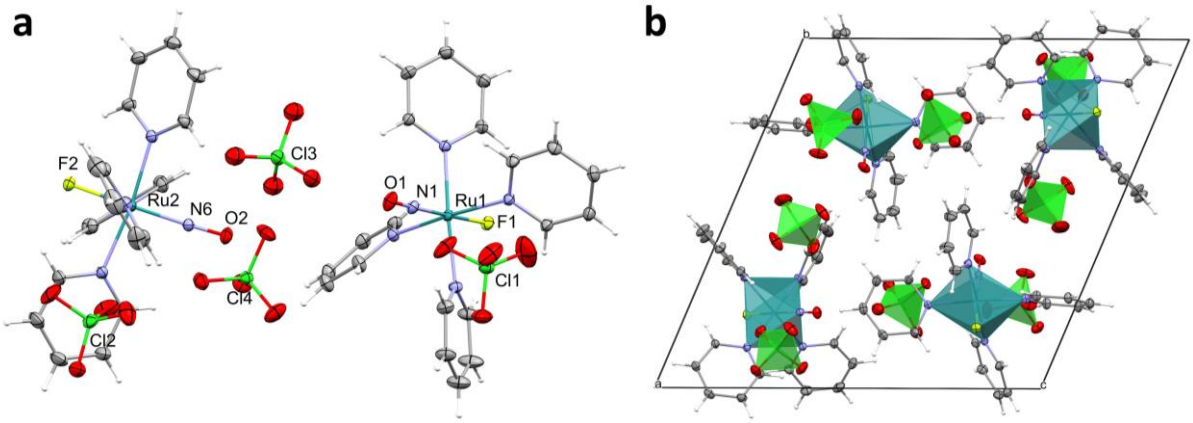

Figure 3 : (a) *ORTEP* plot [37] of complex **I** at 50 % probability ellipsoids at 100 K. The asymmetric unit consist of 6 molecules (Z' = 2): two cations i.e., molecule one with labels Ru1–N1–O1 and molecule two with labels Ru2–N6–O2 and four ClO_4^- anions; (b) crystal packing along *c*-axis.

After having established the GS structure, that is in good agreement with the previously published results [22], we proceeded to the generation of the PLI using the CW and pulsed laser sources. First, we monitored for both cases the generation of MS1 and MS2 by in-situ optical absorption (OA) spectroscopy, as illustrated in Figure 4. These exemplary OA spectra were recorded at 100 K, without collecting the corresponding X-ray diffraction data, in order to speed up the data collection. In this manner we avoid typical problems such as ice formation on the surface of the crystal which can affect the OA spectra significantly or slight repositioning offsets after rotation of the crystal, inducing changes in the baseline. Upon MS1 generation the GS bands in the blue spectral range decrease while a new band centered at around 700 nm arises, a clear signature of MS1, manifest in a color change from light yellow to deep green (see Figure S2). During the transfer from MS1 to MS2 with infrared light (940 nm in this case) the MS1 band at around 700 nm decreases and a new band at about 560 nm appears, the signature of MS2, characterized by its dark color. These measurements establish that CW and pulsed laser irradiation generate the same optical signature. In the following we discuss the corresponding structures determined by XRD on a new crystal at different time points while monitoring the OA spectra (see Figure 4) during the irradiation procedure. In GS and full MS1 (end of irradiation) for the CW case and at 4 distinct points for pulsed irradiation: GS, after 60, 270 and 570 minutes of irradiation with blue light corresponding to different populations of MS1 and after subsequent irradiation with infrared light for the population of MS2. The data collection parameters and refinement statistics for the GS and final data sets of MS1 and MS2 are given in Table 2. The additional intermediate data sets for MS1 (60 and 270 minutes blue light) are reported in Tables S2-S3.

Table 2: Data collection parameters and refinement statistics for all data sets measured in $[Ru(py)_4(NO)F](ClO_4)_2$ upon CW and pulsed laser irradiation.

[Ru(Py)$_4$(NO)F](ClO$_4$)$_2$	*GS*	*MS1$_{CW}$*	*MS1$_{Pulsed}$*	*MS2$_{CW}$*	*MS2$_{Pulsed}$*
Crystal data					
Chemical formula	$[Ru(NC_5H_5)_4(NO)F](ClO_4)_2$				
Crystal system, space group	Triclinic, *P*-1				
Temperature (K)	100(1)				
a, *b*, *c* (Å)	10.4675(16), 16.445(3), 16.580(6)	10.5338(5), 16.4775(9), 16.4316(8)	10.5583(10), 16.4988(15), 16.3871(15)	10.4672(11), 16.522(2), 16.4946(19)	10.4832(11), 16.4774(15), 16.5948(15)
α, β, γ (°)	66.97(2), 87.13(2), 83.187(14)	65.862(4), 87.597(4), 82.329(4)	65.494(7), 87.581(8), 82.504(7)	66.199(9), 87.064(9), 82.220(9)	65.819(7), 82.857(8), 87.089(8)
V (Å^3)	2602.2(12)	2579.1(2)	2575.0(4)	2585.9(5)	2594.7(5)
Z	4				
Radiation type	Mo *K*α				
μ (mm^{-1})	0.88				
Crystal size (mm^2)	0.1×0.2×0.28	0.1×0.2×0.28	0.2×0.2×0.4	0.1×0.2×0.28	0.2×0.2×0.4
Data collection					
Diffractometer	STOE STADIVARI equipped with RebirX 540S CEGITEK Hybrid Pixel Area Detector (HPAD)				
No. of measured, independent and observed [$I > 2\sigma(I)$] reflections	55128, 22450, 18963	45259, 17114, 15158	45052, 19050, 14803	56230, 22533, 18682	46107, 19168, 14080
R_{int}	0.0144	0.0256	0.0312	0.0207	0.0311
Refinement					
$R[F^2 > 2\sigma(F^2)]$, $wR(F^2)$, S	0.0267, 0.0633, 1.112	0.0381, 0.0817, 1.092	0.0362, 0.0796, 1.087	0.0310, 0.0726, 1.024	0.0404, 0.0934, 1.086
No. of parameters	683	776	764	769	715
$\Delta\rho_{max}$, $\Delta\rho_{min}$ (e Å^{-3})	1.10, -0.93	1.41, -1.18	1.45, -1.70	1.28, -1.24	1.13, -1.59

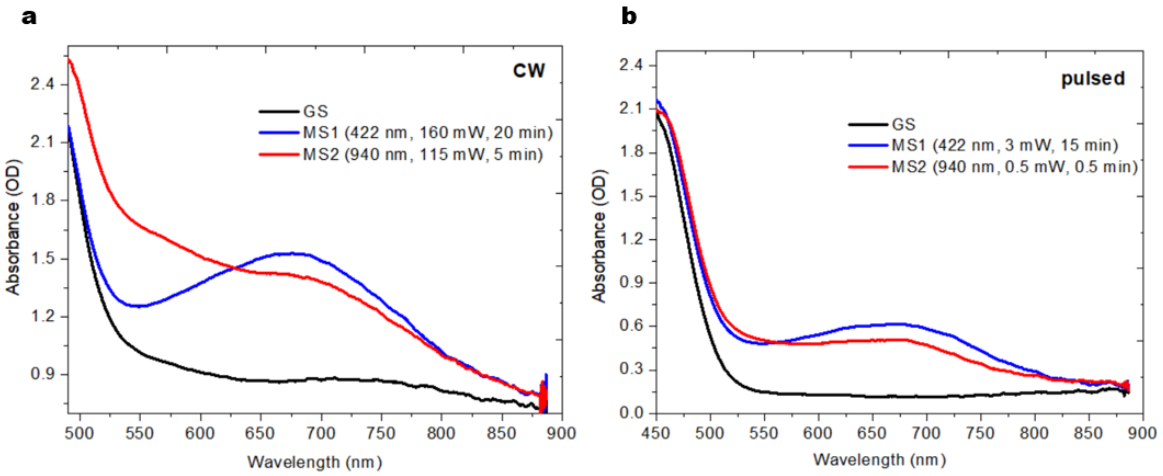

Figure 4: Exemplary OA spectra during PLI (MS1 and MS2) generation in **I** using a single crystal of 200 µm thickness (a) after CW irradiation *P* = 160 mW; *t* = 20 min at 422 nm for generation of MS1 and *P* = 115 mW; *t* = 5 min at 940 nm for transfer to MS2 (b) With pulsed laser MS1 was generated using *P* = 3 mW; *t* = 15 min at 422 nm and transferred to MS2 using *P* = 0.5 mW; *t* = 0.5 min at 940 nm with *f* = 10 Hz.

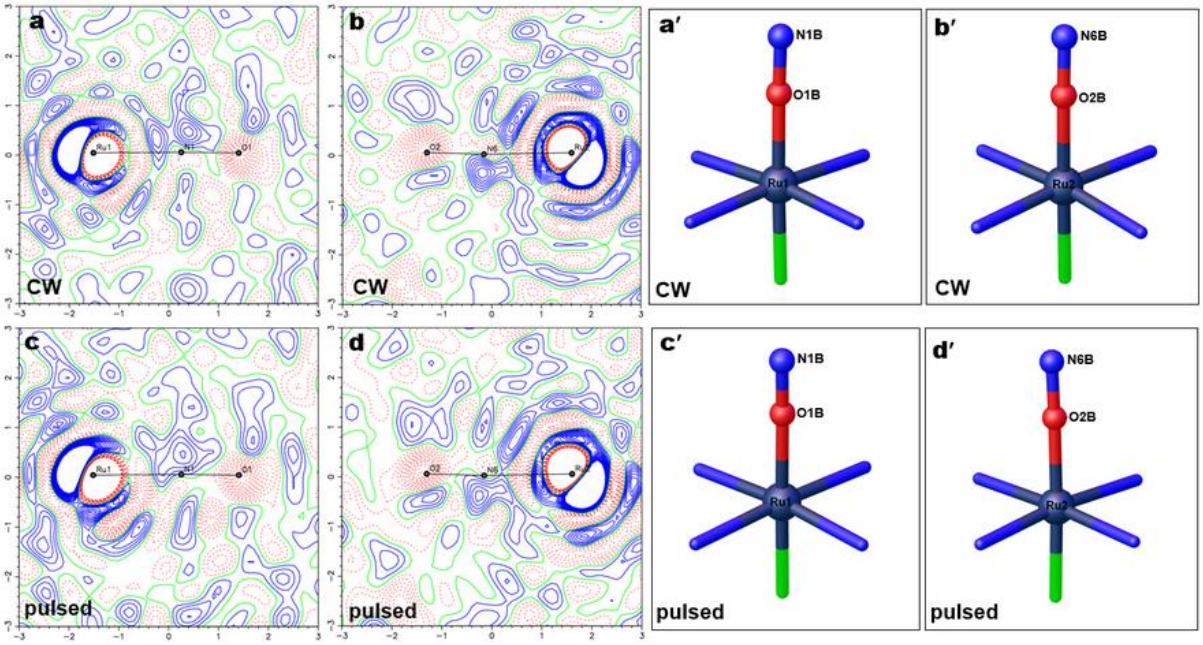

Figure 5: Photodifference maps of **I** after generation of MS1 using CW irradiation (λ = 422 nm, *Q* = 1354 J/cm^2) for (a) molecule one and (b) molecule two and their corresponding structural model are represented in (a') and (b') respectively. After irradiation with 'pulsed laser' the photodifference maps of (c) molecule one and (d) molecule two, and the corresponding structural model in (c') and (d'). In photodifference maps the blue/solid line = +ve, red/dashed line = -ve and green = 0 and the contours level of all the maps are 0.4 eÅ^{-3}. The maximum and minimum electron density recorded from structural refinements of MS1 is 1.41, -1.18 in CW and 1.45, -1.70 in case of irradiation with pulsed laser.

First, we proceed to the analysis of the PLI generated by CW irradiation, which serves as a reference to compare with the already published results, but with the advantage that we performed all the experiments on the same diffractometer and using the same data reduction software as will be the case for the data obtained from pulsed irradiation.

For the population of MS1 a CW laser of 422 nm wavelength was used with an average power of P = 120 mW on a surface of A = 0.478 cm^2, yielding 250.8 mW/cm^2, for a total duration of 90 minutes with a Q value of 1354 J/cm^2. X-ray diffraction data was collected, and photodifference maps were calculated (see Fig. 5a, b). The photodifference map (see supplementary S2.1) is a tool for the first unbiased look to qualitatively assess the photoinduced structural changes by using common independent reflections between the GS and photo-irradiated state by the inverse Fourier transform of the difference, while using the phases obtained from the reference GS structural model (see supplementary information and references [38,39] for more detail). The photodifference maps shows the typical features for the isonitrosyl PLI, a depletion of electron density on the GS positions O1 and O2, and some additional electron density around the N1 and N6 positions in both independent molecules of **I**. The corresponding structural model (see Fig. 5a',b', Table 3) was refined, resulting in a population of 81(2) % for molecule 1 and 89(2) % for molecule 2, in reasonable agreement with published data [22]. The refinement details are presented in supplementary material section S2.2.

In a second step, MS2 was generated from MS1 by irradiation with 940 nm wavelength from a CW source (Thorlabs LED M940L3), with P = 200 mW for t = 60 min, yielding Q = 923 J/cm^2. The photodifference maps (Fig. 6 a,b) show the typical features of the side-on nitrosyl configuration, a depletion on the GS NO positions, and new electron density peaks at about 90° orientation with respect to the GS structure. The structural refinement yielded an MS2 structure with a population of MS2 of 15(1) % for molecule 1 and no refinable population for molecule 2 (see Fig. 6a', b' and Table 3), in agreement with the earlier report [22]. The results of the structural refinements and corresponding statistics are given in Table 3 and in comparison, with GS and MS1 we find that the structures agree with those published [22]. Another crystal of $[Ru(Py)_4(NO)F](ClO_4)_2$ was used for the study of MS1 and MS2 generated by pulsed laser irradiation.

Having confirmed that the structures of MS1 and MS2 obtained from CW irradiation correspond to the previously published ones, we proceeded to the generation of these PLI by pulsed Laser irradiation. For the population of MS1, we used the same wavelength as for the CW study, 422 nm, but this time using the EKSPLA pulsed laser (f = 10 Hz; ≈ 5 ns pulse duration) and adjusted the average power to P = 2.5 mW, corresponding to an average intensity on the crystal of I = 35 mW/cm^2. Irradiation was performed for a total duration of 570 minutes, yielding a total fluence of Q = 1197 J/cm^2. One minute of pulsed laser irradiation corresponds to 600 laser pulses, so after 570 minutes the crystal was irradiated with 342'000 laser pulses. Three X-ray data sets MS1A, MS1B and MS1C (or $MS1_{Pulsed}$) were collected after 60, 280, and 570 minutes, corresponding to Q values of 126, 588, and 1197 J/cm^2. We will concentrate here on the final MS1 structure i.e., MS1C, at Q = 1197 J/cm^2 for comparison with the CW measurement. We refer the reader to Tables S2, S3 for the description of the structures of MS1A, MS1B. The increase of the MS1 population was again monitored by collecting OA spectra (11 time points in total, see Figure S3 b). Fig. 5 c, d shows the corresponding photodifference maps exhibiting the features typical for the isonitrosyl PLI: a depletion of electron density on the oxygen position of NO and an accumulation around the nitrogen position of NO. The corresponding structural models have been refined, and the results are listed in Table 3. The refined populations amount to 85(2) and 87(2) % for molecules 1 and 2, respectively.

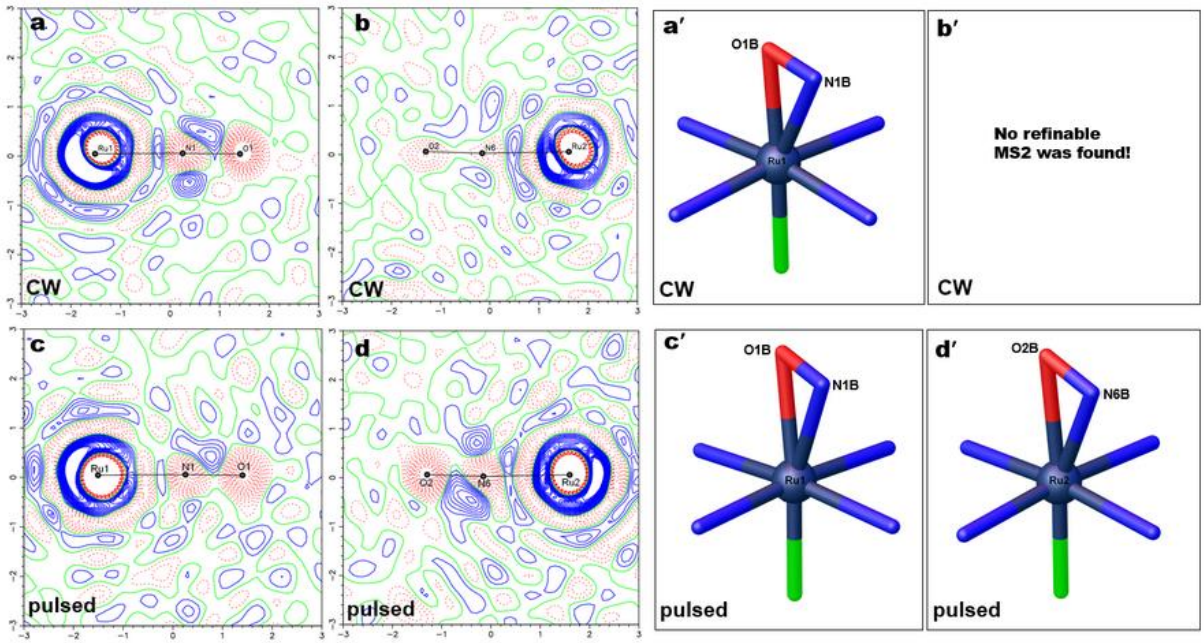

Figure 6: Photodifference maps after generation of MS2 using CW irradiation (940 nm, Q = 923 J/cm^2) for (a) molecule one and (b) molecule two, and the corresponding structural model in (a') for molecule one, while (b') no refinable structural model was found for the case of molecule two. After irradiation with 'pulsed laser' the photodifference maps of (c) molecule one and (d) molecule two, and the corresponding structural model in (c') and (d'). In photodifference maps the blue/solid line = +ve, red/dashed line = -ve and green = 0 and the contour levels for all the maps are 0.3 eÅ^{-3}. The maximum and minimum electron density recorded from structural refinements of MS2 is 1.28, -1.24 in CW and 1.13, -1.59 in case of irradiation with pulsed laser.

Comparing the structural models obtained for MS1 we note that the photoconversion is the same, independent of the used irradiation source. The Ru1–O1B and Ru2–O2B distances are 1.861(3) Å and 1.854(3) Å in the case of CW irradiation, and 1.865(3) Å and 1.855(3) Å in the case of pulsed irradiation i.e., 0.004 and 0.001 % relative changes. The corresponding Ru–O–N angles show small differences (max difference is 0.9°).

The two other data sets for MS1 collected after 60 and 280 minutes of irradiation, corresponding to Q = 126 and 588 J/cm^2, were refined accordingly. The populations found for MS1 in molecules 1/2 are 26(2)/15(2) % and 69(2)/60(3) % (see Figure S4 depicting corresponding photodifference maps). Knowing these populations of MS1A–C, we can fit $P(Q) = P_{max}(1\text{-}\exp(-Q/Q_0)$, yielding Q_0 = 450(200) J/cm^2 and P_{max} = 91(16) %, as illustrated in Figure S6. This fit confirms the overall monoexponential population kinetics, even though the errors are rather large due to the few data points and the overall long measurement time including collection of four XRD data sets.

For the population of MS2 (transfer starting from MS1), we used the same wavelength as for the CW study, 940 nm, and EKSPLA pulse laser (f = 10 Hz), with adjustment of average power to P = 2 mW. This corresponds to intensity on the crystal of I = 28mW/cm^2 (d of spot size = 0.3 cm). Irradiation was performed for a total duration of 120 minutes, yielding a total fluence of Q = 202 J/cm^2.

The structural analysis follows the usual procedure. From the photodifference maps we can again clearly identify the features of the side-on nitrosyl configuration, this time with clear differences for both of the two molecules in the unit cell. The corresponding refinement statistics of the MS2 model and its parameters are given in Table 3. Fig. 6c', d' illustrates the result for the structural model of MS2.

From CW to pulsed data of MS2, the percentage relative changes observed in bond distances and bond angles of molecule one is small. In molecule 1, the obtained structure corresponds to the one published [22]. Interestingly, for molecule 2, we found an MS2 side-on structure as well with a similar population as for molecule 1. There is, thus a significant difference to the CW results, where no MS2 was found for molecule 2. The most probable origin for this difference is the fact that we use two different light sources for the generation of MS2. In the CW experiment, starting from MS1, we transfer by LED light, while for the pulsed experiment, we use the laser line from the OPO. The LED light is not monochromatic, contrary to the laser light, which has a comparatively narrower bandwidth. Looking at the emission spectrum of the Thorlabs M940L3 LED, we find quite a large bandwidth centred around 940 nm, with a rather long tail in the high energy side, down to almost 800 nm. It seems that for **I**, the two molecules of the unit cell have slightly different absorption properties, which leads to the depopulation of molecule 2 when irradiated with the broad-band LED. When using the narrower laser line at 940 nm, MS2 can be produced in both molecules. If one would do a systematic study of this transfer as a function of wavelength (using the OPO for finely tuning the wavelength) one could therefore probably detect the differences in the absorption spectra of the two molecules.

Table 3: Main structural parameters obtained from refinement of GS and MS1 and MS2 for various data sets.

Bond length [Å]/ Angle [°]	*GS*	$MS1_{CW}$	$MS1_{Pulsed}$	$MS2_{CW}$	$MS2_{Pulsed}$
Ru1—N1	1.768(1)	-	-	-	-
Ru1—O1B	-	1.861(3)	1.865(3)	2.15(1)	2.19(3)
Ru2—N6	1.760(1)	-	-	-	-
Ru2 – O2B	-	1.854(3)	1.855(3)	-	2.11(2)
Ru1—F1	1.933(1)	1.912(1)	1.908(1)	1.927(1)	1.921(2)
Ru2—F2	1.927(1)	1.905(1)	1.904(1)	1.919(1)	1.917(2)
N1—O1	1.153(1)	-	-	-	-
N1B—O1B	-	1.166(5)	1.169(5)	1.15(1)	0.97(3)
N6—O2	1.149(1)	-	-	-	-
N6B—O2B	-	1.155(4)	1.155(4)	-	1.06(3)
Ru1—N1—O1	179.0(1)	-	-	-	-
Ru1—O1B—N1B O1B—Ru1—N1B	- -	176.3(9) -	177.2(8) -	68.2(7) 31.8(3)	64(3) 26(1)
Ru2—N6—O2	177.3(1)	-	-	-	-
Ru2—O2B—N6B O2B—Ru2—N6B	- -	176.1(7) -	175.7(7) -	- -	70(2) 30(1)
Population [%]					
PLI(Mol. 1) GS(Mol. 1) PLI(Mol. 2) GS(Mol. 2)		81(2) 19(2) 89(2) 11(2)	85(2) 15(2) 87(2) 13(2)	15(1) 85(1) Not Found!	19(1) 81(1) 14(1) 86(1)

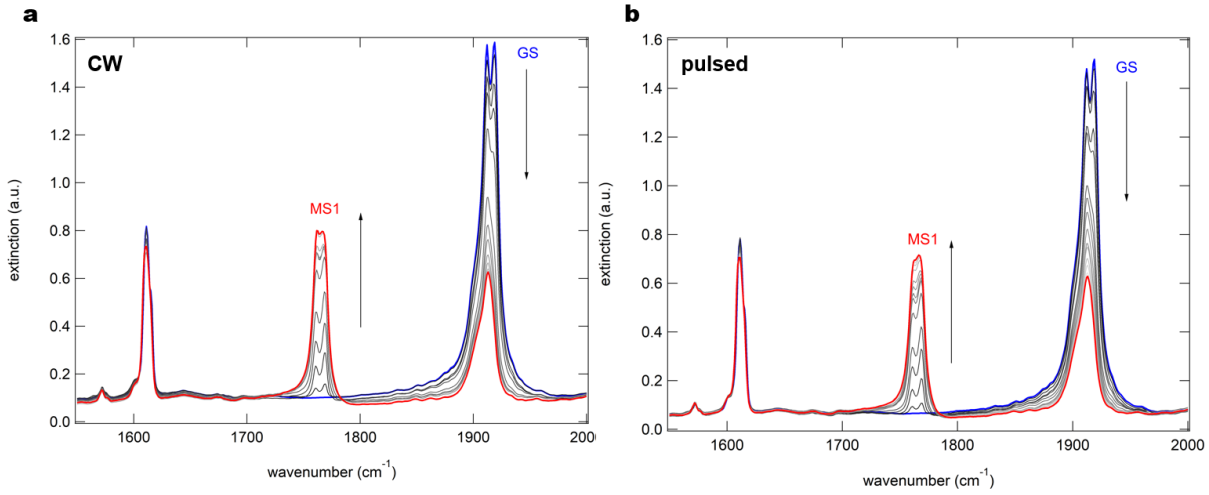

Figure 7: MS1 generation in **I**. upon (a) CW and (b) pulsed laser irradiation. The population of MS1 can be calculated from the decrease of the GS band area.

The XRD and in-situ OA results clearly show that at low temperature the MS1 and MS2 generated by CW and pulsed irradiation are identical. Moreover, in both cases we find exclusively MS1 after blue light irradiation, while MS2 needs to be generated by infrared light out of MS1. These two measurements are thus not sufficiently sensitive to identify a possible presence of MS2 during the population of MS1, as is expected from the two-step mechanism for its generation. We therefore investigated the population behaviour of MS1 by infrared spectroscopy using the two types of irradiation sources. IR spectroscopy allows to identify the GS, MS1, and MS2 species due to their distinct ν(NO) vibration at 1912/1918 cm^{-1}, 1761/1768 cm^{-1}, and 1565/1597 cm^{-1} for GS, MS1, and MS2, respectively. Fig. 7 shows the results, when using 422 nm as irradiation wavelength and using 1.6 mg of **I** diluted in 1.6 mg of KBr. Average intensity was 108.7 mW/cm^2 for CW and 84 mW/cm^2 for pulsed irradiation. Total irradiation time was 60 and 90 minutes for CW and pulsed irradiation, respectively.

Plotting the population, calculated from the decrease of the GS band area at 1912/1918 cm^{-1}, as a function of fluence we can obtain the characteristic value for achieving the saturation, and a comparison of the kinetics of population between pulsed and CW irradiation. Both types of irradiation result in the same mono-exponential increase with a characteristic constant of 112(6) J/cm^2 and 109(4) J/cm^2 for CW and pulsed irradiation, respectively. The obtained populations amount to 73(2) % for CW and 65(2) % for pulsed irradiation. We note that during the experiment, with increasing exposure to light, first CW and then pulsed on the same sample, some NO release is observed, for a total amount of 5 %.

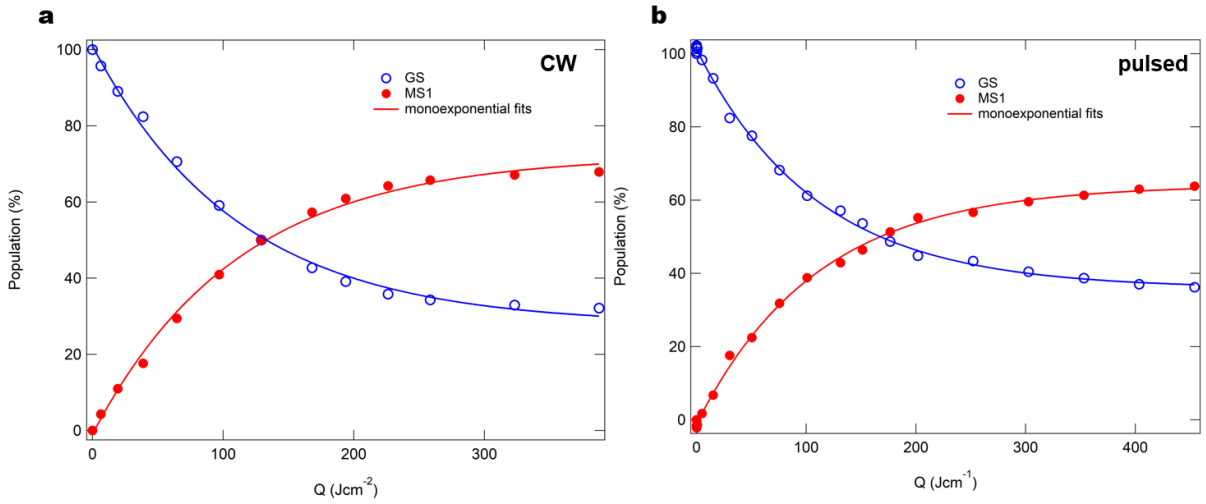

Figure 8 : MS1 population as a function of fluence in **I** upon (a) CW and (b) pulsed laser irradiation. The population shows a monoexponentially increase with a time constant of 112(6) J/cm^2 for CW and 109(4) J/cm^2 for pulsed irradiation.

Let us calculate the number of photons necessary to achieve saturation population, for a *Q*-value of about 400 J/cm^2 in the case of the diluted sample in a KBr pellet. **I** has a molar mass of 665.37 g/mol, hence 1.6 mg correspond to 2.404677 × 10^{-6} mol or 1.448 × 10^{18} molecules in the pellet. The irradiated surface of the KBr pellet is 1.326 cm^2, so the total energy on the pellet is 530.4 J, corresponding to 1.12678 × 10^{21} photons. There are thus about 780 photons per molecule and with this amount one reaches about 70 % of population of MS1. This implies that the overall switching efficiency from GS to MS1 is about 0.1 %. Note that this overall switching efficiency calculated for obtaining the saturation population includes the absorption properties of GS, MS1 (and MS2 if it is a two-step process), as well as the corresponding probabilities to induce the forward and backward processes. Therefore, it does not correspond to the efficiency of a single switching process, but to an average value over the whole irradiation time resulting in the photo-stationary equilibrium. By comparing this value from IR experiment to the one obtained in the XRD experiment, where saturation is obtained for about 1200 J/cm^2, corresponding to 1.01 ×10^{18} photons on its surface of approximately 0.02 × 0.02 cm^2. In the crystal of (approximate) dimension 0.02 × 0.02 × 0.02 cm^3 there are 6.19 ×10^{15} molecules, yielding an overall switching efficiency of 0.6 %. This is slightly higher than for the IR measurement (allowing for an error of a factor of two). So, even though the calculated optical thickness of the KBr pellet is 14 times less than the one of the single crystals used for XRD, the crystal provides a better overall switching efficiency, most probably because a crystal offers an optically perfect surface, while the KBr matrix results in the diffusion of the laser light. On the other hand, the larger Q-value necessary for achieving saturation population in the XRD experiment is due to this higher optical thickness. The absorption coefficient α at 422 nm is about 80 cm^{-1}, as can be calculated from the absorbance $A = \alpha d$ with the given thickness of 0.02 cm. This results in a damping of the incoming intensity to 20 % after passing through the crystal.

Coming back to the IR experiment, and the question whether the signature of MS2 is visible in these spectra, we zoom into the spectra after only a few pulses at 422 nm (Fig. 9a). While at first sight only MS1 is generated, the difference spectra between the irradiated sample and the GS after 1, 10, 20, 50, and 100 pulses and then after 1, 3 and 10-minutes reveal indeed the presence of MS2. After 10 pulses a signature of MS2 is visible which then steadily increases until about 3 minutes before decreasing again. MS1 becomes only visible after 100 pulses. Clearly MS2 is generated first and is transferred with increasing number of pulses towards MS1, so that at the end only MS1 remains, with a transient

population of MS2 staying at 1 % or below. This observation clearly confirms the two-step mechanism postulated earlier [22,27]. The corresponding mechanistic scheme is shown in Fig. 9b.

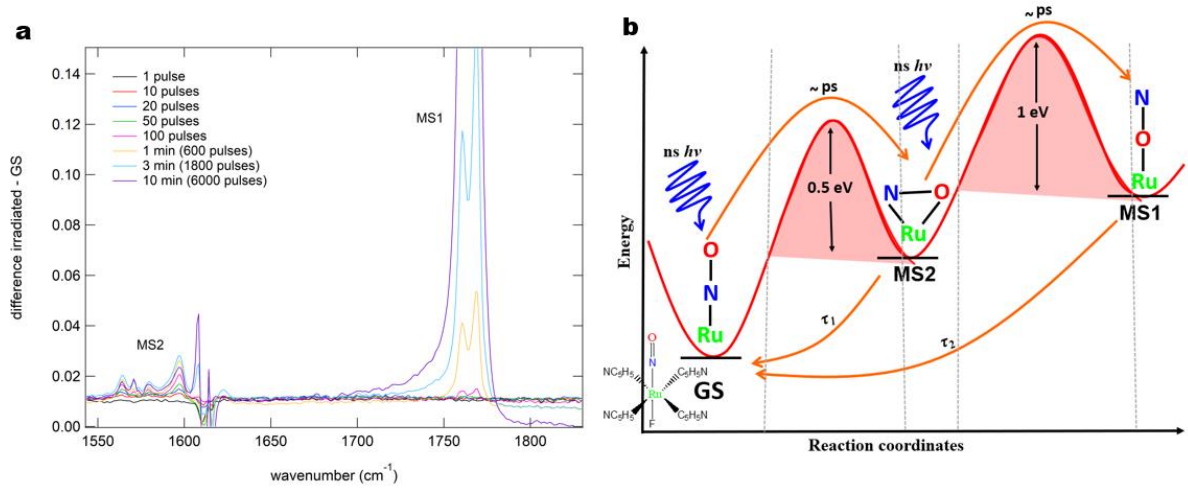

Figure 9: Difference spectra at 100 K between irradiated sample (pulsed laser) and GS, illustrating the increase of MS2, visible after 10 pulses, and later MS1, visible after 100 pulses.

Conclusions

The influence of the type of photo-irradiation source on the generation of PLI in a $\{MNO\}^6$ type ruthenium-mononitrosyl complex $[Ru(Py)_4(NO)F](ClO_4)_2$ (**I**) has been investigated by XRD, UV/Vis and IR spectroscopy, and the overall switching efficiency has been quantified in terms of effective number of photons required to achieve the photo-stationary state at a particular temperature (excluding thermally activated relaxation). In conclusion, we can state that by pulsed laser irradiation at low temperatures in steady-state conditions, we reproduced the same results as by CW irradiation concerning the structures and population of MS1 and MS2 in **I**. For MS2, there are some differences, which are not related to the temporal difference of the CW/pulsed light source but to their different spectral bandwidth. For **I** the pulsed experiments showed that the transfer to MS2 for the two independent molecules in the unit cell depends on the wavelength, and the pulsed laser light offers an opportunity to study this effect in more detail. Overall, we confirm that pulsed excitation produces the same MS1 and MS2 structures as CW irradiation at low temperatures. This is an important result as it shows that by nanosecond laser excitation, the same PLI are generated than with CW laser irradiation. Hence, time-resolved studies will be addressing the same PLI and yield insight in the corresponding generation and relaxation pathways. From a methodological point of view, we have seen that the OA spectra allow to quickly (in a few minutes the crystal is aligned, and the spectrum was collected) obtain information whether population of the crystal has succeeded or not. This is a significant advantage for such photocrystallographic studies because the X-ray data collection takes many hours, in particular for low-symmetry crystals.

Further, knowing the population, either from OA measurements or the XRD refinement, the ratio of photons to number of switched molecules can be calculated. The number of photons required to achieve saturation population is the same in CW and pulsed irradiation, and hence one can either increase intensity or irradiation time in order to reach the needed *Q*-value. This opens the way for ultrafast pump-probe studies, where a maximum amount of population is desirable and should be induced by a single laser pulse and therefore to investigate the photoswitching mechanism. The only limitation is then the damage threshold of the crystal under study.

Finally, the monitoring of the IR spectra upon step-by-step pulsed population of MS1 revealed the presence of MS2 during the MS1 generation. As a matter of fact, the MS2 is generated first, before being transferred to MS1, thereby confirming the two-step model for the generation of MS1. Since the population of MS2 during this process remains below 1 %, it was not detected in the X-ray or OA measurements on single crystals.

Acknowledgements

A. H. thanks Région Grand Est for financial support (Project Number19_GE6_108). We acknowledge financial support from ANR (grant ANR-21-CE30-0045-01), CPER (projects MATDS and SusChemProc) The work was carried out using PMD2X X-ray diffraction facility of the Université de Lorraine. We thank E. Wenger for help with XRD data treatment.

Keywords

Continuous wave laser, Metal nitrosyls, Photocrystallography, Photoinduced linkage isomerism, Pulsed laser, two-step mechanism

References

[1] T. Woike, D. Schaniel, Eds. , *Z. Für Krist. - Cryst. Mater.* **2008**, *223*, IV–IV.
[2] P. Coppens, *Angew. Chem. Int. Ed.* **2009**, *48*, 4280–4281.
[3] E. Collet, *Acta Crystallogr. A* **2010**, *66*, 133–134.
[4] P. Naumov, in *Adv. X-Ray Crystallogr.* (Ed.: K. Rissanen), Springer Berlin Heidelberg, Berlin, Heidelberg, **2011**, pp. 111–131.
[5] M. Huber, *Angew. Chem. Int. Ed.* **1998**, *37*, 1073–1075.
[6] K. Sokolowski-Tinten, D. von der Linde, *J. Phys. Condens. Matter* **2004**, *16*, R1517–R1536.
[7] S. Ohkoshi, H. Tokoro, *Acc. Chem. Res.* **2012**, *45*, 1749–1758.
[8] O. Sato, *Acc. Chem. Res.* **2003**, *36*, 692–700.
[9] W. Xu, S. Sun, S. Wu, *Angew. Chem. Int. Ed.* **2019**, *58*, 9712–9740.
[10] D. Bléger, S. Hecht, *Angew. Chem. Int. Ed.* **2015**, *54*, 11338–11349.
[11] M. Irie, T. Fukaminato, K. Matsuda, S. Kobatake, *Chem. Rev.* **2014**, *114*, 12174–12277.
[12] L. E. Hatcher, M. R. Warren, J. M. Skelton, A. R. Pallipurath, L. K. Saunders, D. R. Allan, P. Hathaway, G. Crevatin, D. Omar, B. H. Williams, B. A. Coulson, C. C. Wilson, P. R. Raithby, *Commun. Chem.* **2022**, *5*, 102.
[13] P. Coppens, I. Novozhilova, A. Kovalevsky, *Chem. Rev.* **2002**, *102*, 861–884.
[14] D. Schaniel, Th. Woike, J. Schefer, V. Petříček, *Phys. Rev. B* **2005**, *71*, 174112.
[15] P. Naumov, P. Makreski, G. Jovanovski, *Inorg. Chem.* **2007**, *46*, 10624–10631.
[16] Y. Ohashi, in *Cryst. State Photoreact.*, Springer Japan, Tokyo, **2014**, pp. 83–124.
[17] L. E. Hatcher, J. M. Skelton, M. R. Warren, P. R. Raithby, *Acc. Chem. Res.* **2019**, *52*, 1079–1088.
[18] J. M. Cole, D. J. Gosztola, S. O. Sylvester, *RSC Adv.* **2021**, *11*, 13183–13192.
[19] K. A. Deresz, R. Kamiński, S. E. Kutniewska, A. Krówczyński, D. Schaniel, K. N. Jarzembska, *Chem. Commun.* **2022**, *58*, 13439–13442.
[20] J. H. Enemark, R. D. Feltham, *Coord. Chem. Rev.* **1974**, *13*, 339–406.
[21] A. Hasil, D. Beck, D. Schröder, S. Pillet, E. Wenger, T. Woike, P. Klüfers, D. Schaniel, *Angew. Chem. Int. Ed.* **2022**, *61*, DOI 10.1002/anie.202210671.
[22] A. A. Mikhailov, E. Wenger, G. A. Kostin, D. Schaniel, *Chem. – Eur. J.* **2019**, *25*, 7569–7574.
[23] B. Cormary, I. Malfant, M. Buron-Le Cointe, L. Toupet, B. Delley, D. Schaniel, N. Mockus, T. Woike, K. Fejfarová, V. Petříček, M. Dušek, *Acta Crystallogr. B* **2009**, *65*, 612–623.
[24] J. Sanz García, F. Alary, M. Boggio-Pasqua, I. M. Dixon, I. Malfant, J.-L. Heully, *Inorg. Chem.* **2015**, *54*, 8310–8318.
[25] F. Talotta, M. Boggio-Pasqua, L. González, *Chem. – Eur. J.* **2020**, *26*, 11522–11528.
[26] F. Talotta, J.-L. Heully, F. Alary, I. M. Dixon, L. González, M. Boggio-Pasqua, *J. Chem. Theory Comput.* **2017**, *13*, 6120–6130.
[27] L. Khadeeva, W. Kaszub, M. Lorenc, I. Malfant, M. Buron-Le Cointe, *Inorg. Chem.* **2016**, *55*, 4117–4123.
[28] A. Gansmüller, A. A. Mikhailov, G. A. Kostin, J. Raya, C. Palin, T. Woike, D. Schaniel, *Anal. Chem.* **2022**, *94*, 4474–4483.
[29] K. A. Konieczny, A. Hasil, M. Deutsch, C. Palin, D. Schaniel, S. Pillet, *Submiss.* **2023**.
[30] Stoe and Cie, **2018**.
[31] G. M. Sheldrick, *Acta Crystallogr. Sect. Found. Adv.* **2015**, *71*, 3–8.
[32] G. M. Sheldrick, *Acta Crystallogr. Sect. C Struct. Chem.* **2015**, *71*, 3–8.
[33] O. V. Dolomanov, L. J. Bourhis, R. J. Gildea, J. A. K. Howard, H. Puschmann, *J. Appl. Crystallogr.* **2009**, *42*, 339–341.
[34] F. H. Allen, I. J. Bruno, *Acta Crystallogr. B* **2010**, *66*, 380–386.
[35] D. Schaniel, J. Schefer, B. Delley, M. Imlau, Th. Woike, *Phys. Rev. B* **2002**, *66*, 085103.
[36] A. A. Mikhailov, T. Woike, A. Gansmüller, D. Schaniel, G. A. Kostin, *Spectrochim. Acta. A. Mol. Biomol. Spectrosc.* **2021**, *263*, 120217.

[37] L. J. Farrugia, *J. Appl. Crystallogr.* **2012**, *45*, 849–854.
[38] S. Pillet, in *Struct. Differ. Time Scales*, De Gruyter, **2018**, pp. 143–219.
[39] A. Hasil, Dynamique Structurale de Complexes Photoisomérisables : De La Seconde à La Femtoseconde, Université de Lorraine, **2022**.

Supporting Information

CW or Pulsed laser — That is the Question: Comparative Steady-state Photocrystallographic Analysis of Metal Nitrosyl Linkage Isomers

S1 Characteristics of the photo-irradiation sources: CW and pulsed laser

In order to compare the effect of CW or pulsed irradiation, we first have a look at the output of CW and pulsed lasers. As schematically illustrated in Figure 1 (main text), a CW laser provides a constant power output P_{avg} (given in Watts). The total energy seen by the sample, can be calculated by multiplying this constant output P_{avg} with the time during which the sample was irradiated.

$$E_{CW} = P_{avg} \times t_{irradiation} \quad \text{(S1)}$$

If the spot size of the laser beam (area A) is known, we can calculate the energy density (Joules per square meters) as:

$$e_{CW} = {}^{E_{CW}}/_{A} \quad \text{(S2)}$$

However, careful attention is needed since in general, laser beams do not exhibit a flat-top profile but rather Gaussian shapes; the energy density is not homogeneous over the spot size. To accurately determine the (spatial) peak energy density being delivered to a material in a (pulsed) laser experiment, the shape and distribution of the (pulse) laser beam must be considered. We will not consider this aspect of spatial beam profile further here. In most of the experiments, in general, we use expanded laser beams, to make sure that beam size is larger than the sample size and thereby, considering the spatial beam profile on the sample position as flat-top, which results in a constant energy density over the irradiated area.

In the case of a pulsed laser, the energy delivered by the laser is concentrated in (short) pulses, arriving on the sample at a given frequency f (repetition rate of laser) with a temporal peak shape Figure 1 (main text) often considered to be of Gaussian type with a full width at half maximum (FWHM) corresponding to the so-called pulse duration τ_{pulse}. The average power P_{avg} is then linked $P_{avg} = E_{pulse} \times f$ to the pulse energy by:

$$E_{pulse} = {}^{P_{avg}}\Big/_{f} \quad \text{(S3)}$$

e.g., for a 10 Hz repetition rate and a pulse energy of 10 mJ, an average power of 100 mW is obtained. The peak power of the pulse depends on the temporal peak shape. For a rectangular peak shape, it is simply the pulse energy divided by the pulse duration $P_{peak\,rect} = {}^{E_{pulse}}/_{\tau_{pulse}}$. For a pulse with Gaussian shape, one has $P_{peak\,gauss} = {}^{2\sqrt{\log(2)/\pi} \times E_{pulse}}\Big/_{\tau_{pulse}}$. Note that this is due to the Gaussian shape, one has $P_{peak\,gauss} = {}^{2\sqrt{\log(2)/\pi} \times E_{pulse}}\Big/_{\tau_{pulse}}$. Note that this is due to the Gausssian peak shape in time, we still consider the spatial peak shape as flat-top since we place the sample in the expanded beam, leading to a homogeneous (spatial) energy density.

The population of photo-switched molecules depends on several factors, notably the cross-sections for the forward GS-to-PLI process and the backward PLI-to-GS process at the excitation wavelength (in steady-state conditions). In an ideal case, there would be only the forward process, and the switching

efficiency would be 100 % if the quantum yield is considered as one. Under these conditions, the number of photons to number of molecules ratio can be calculated after laser irradiation. If one absorbed photon is effective to switch one molecule after laser irradiation, then we can estimate the minimum number of photons required to switch 100 % of the molecules in a given crystal volume. The number of photons $n_{photons}$ in a laser beam of energy E_{laser} is given by:

$$E_{laser} = n_{photons}\frac{hc}{\lambda} \tag{S4}$$

with the Planck constant h = 6.62607015×10^{-34} Js, c = 299792458 ms^{-1} the speed of light, and λ the wavelength of the laser light. The corresponding energy density e_{laser} is given by:

$$e_{laser} = \frac{E_{laser}}{A} \tag{S5}$$

with A the reference surface used for determining the energy density. If we now shine the laser beam on a crystal with surface area $A_{crystal}$, the energy contained in this area of the laser beam is given by:

$$E_{laser\ on\ crystal} = e_{laser}A_{crystal} \tag{S6}$$

So that we end up with the number of photons entering on a crystal with surface $A_{crystal}$

$$n_{photons\ on\ crystal\ surface} = \frac{e_{laser}A_{crystal}}{hc} \tag{S7}$$

Knowing the energy density (or fluence) for CW lasers $e_{CW} = {P_{avg} \times t}/{A}$ and for pulsed lasers $e_{pulse} = {P_{avg}}/{(f \times A)}$ the number of photons impinging on the crystal can be calculated for the two cases as a function of the chosen irradiation strategy.

In case of irradiation for a given time Δt (long with respect to the pulse duration and the inverse of f) the energy density is $e_{laser} = {P_{avg} \times \Delta t}/{A}$ for both cases. The difference lies in the fact that the CW laser irradiation is constant over time thus leading to a linear increase of the total number of photons which have arrived on the crystal, while the pulsed laser irradiation is a succession of short bursts of pulses containing many photons, separated by comparatively long times with no photons at all. For example, for an average power of 100 mW at a wavelength of 422 nm, a beam size of 500 micrometer diameter and a crystal size of 200 x 200 micrometer, an energy density of 50.9424 W/cm^2 is obtained and the corresponding number of photons on the crystal is 2.42345 x 10^{16} in 1 second. The CW laser brings in a steady flow of photons equally distributed over time, the pulsed laser on the other hand, compresses this number of photons into short bursts. For example, a nanosecond pulsed laser with a FWHM of 5 ns, and a repetition rate of 10 Hz, condenses this number of photons into 10 very short pulses, the peak power is then 698'578 W, and the number of photons arriving on the crystal within 5 ns is 2.42345x10^{15}. The pulse laser brings in the same number of photons as the CW laser, but in 1/20'000'000 of the time. In that manner the same number of photons is found in one single pulse of 5 ns compared to the 100 ms of the CW laser (when using the same average power).

In order to estimate whether the number of photons is sufficient for excitation of a majority of molecules present in the probed crystal volume $V_{crystal}$, the number of molecules $Z_{molecules}$ in the crystal can be determined as:

$$Z_{molecules} = \frac{V_{crystal}Z_{unit\ cell}}{V_{unit\ cell}} \tag{S8}$$

where $Z_{unit\ cell}$ is the number of photoswitchable molecules per unit cell, and $V_{unit\ cell}$ is the unit cell volume. So, we should make sure that $n_{photons\ on\ crystal\ surface} > Z_{molecules}$ in order to have a reasonable chance of detecting some molecules in the photoswitched configuration, primarily if we use only a single laser pulse. In steady-state conditions, when the photoswitched molecules remain in their configuration, the number of pulses required to obtain a sufficient number of photons for achieving photo-saturation can be calculated. This is important, as we also have to consider some serious drawbacks of the pulsed laser excitation, such as the potentially significant heating of the crystal, with all kinds of after-effects (rapid crystal damage, photo-bleaching, etc.).

The maximum photoconversion can be achieved after a certain fluence saturation value Q_{sat}, corresponding to the energy density and hence the number of photons necessary to reach this photo-stationary state.

$$Q = I \times t_{irr}\ ;\ Q = \frac{P_{avg}}{A} \times t_{irr} \tag{S9}$$

The saturation value depends on many physical parameters; the quantum efficiency of the switching process, the ratio of the forward and backward processes potentially possible at the given wavelength (depending on the absorption coefficient ∝), as well as the rate of a potential thermal relaxation of the photoinduced species at a given temperature, by the absorption properties of a material, wavelength of laser and optical path. There are additional experiment specific parameters, such as the crystal thickness, the laser power, and irradiation time, which can affect Q_{sat}.

The penetration depth of a laser is another important parameter to take into account that how deeply the laser light, whether its CW or pulsed light source, can penetrate into the crystal or pellet. The penetration depth can be determined by the absorption properties of the material and the wavelength of laser using Beer-Lamber law:

$$I_t = I_0 . e^{-\alpha d} \tag{S10}$$

Where I_0 is the initial intensity of laser, I_t is the transmitted intensity as it passes through the sample, ∝ is the absorption coefficient of the sample and *d* is the optical path length of the material. Using the Eq. S10, the absorption coefficient α can be deduced as follows:

$$\alpha = \frac{1}{d} \ln \left(\frac{I_0}{I_t} \right) \tag{S11}$$

So, the penetration depth (*d*) can be deduced as:

$$d = \frac{1}{\alpha} \ln (A) \tag{S12}$$

This shows that the higher the absorption coefficient αof the sample at a particular wavelength of laser, lower the penetration depth *d* will be (i.e., only on the crystal surface) and vice-versa.

If a crystal is too thick with respect to the absorption coefficient (α), Q_{sat} will increase due to the fact that the backside of the crystal sees much less photons which complicates comparison between different experiments using different sample types (e.g., thin pellets with diluted powder for IR and crystals of a few hundred micrometer thickness in XRD or optical experiments), since the intensity used for calculating is not a constant throughout the sample. If the photoswitching process underlies some threshold value, a too low *P* value might result in no population at all, while very high *P* value might lead to additional wanted or unwanted effects, such as two-photon-absorption processes or photobleaching. It is therefore important to investigate the effect of reducing the irradiation time by increasing the average power (if Q_{sat} is a constant), and especially by significantly increasing the peak

power as is the case for nano- or femtosecond lasers, which can lead to damage, but which on the other hand can open the way to single-shot experiments.

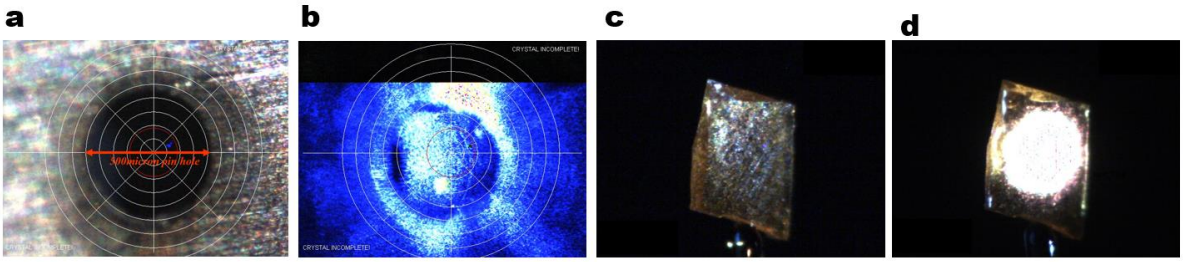

Figure S1: Pin hole 500 µm used for irradiation of crystal for pulsed laser alignment (a), and crystal irradiation with 422 nm pulsed laser (b). Crystal choice for the optical absorption spectral mapping (c) and the spot size of the transmitted light (d) from the crystal to the spectrophotometer detector.

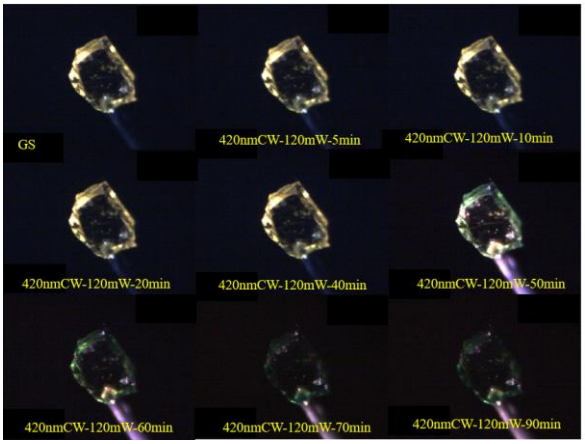

Figure S2: Illustration of colour change in **I** upon irradiation with 422nm CW laser, inducing the photoconversion from GS to MS1.

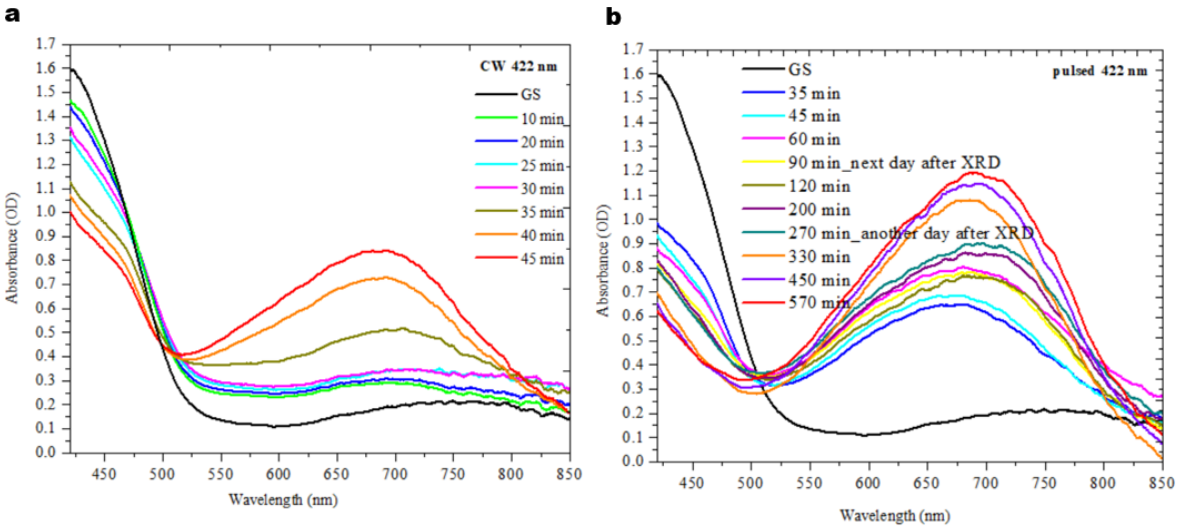

Figure S3: Single crystal OA spectra during MS1 generation in I, the GS band at 450 nm decreases while the band of MS1 at 700 nm arises. (a) OA spectra of MS1 after irradiation with CW, and (b) pulsed laser.

S2 Steady state photocrystallography

S2.1 Photodifference maps:

In X-ray photocrystallography, the first step in the analysis of the data is, in general, to inspect so-called *photodifference maps* (2D or 3D), a useful tool for the first unbiased look to qualitatively assess the photoinduced structural changes. The excitation by light source leads to induce changes in electron density and hence modifies structure. Therefore, a photodifference map is calculated by using '*common'* independent reflections between the ground state GS and the photo-irradiated state PLI by the inverse Fourier transform of the difference while using the phases obtained from the refinement of the reference GS structural model. As a first approximation, the phases for the photo-irradiated state (composed of GS and PLI fractions) are assumed to be the same as those of the pure ground state and are thus calculated from the ground state structural model.

$$F^{obs}_{photodifference}(hkl) = F^{obs}_{ES}(hkl) - F^{obs}_{GS}(hkl) \quad \text{(S13)}$$

$$\Delta\rho^{obs}_{photodifference}(hkl) = \rho^{obs}_{ES}(hkl) - \rho^{obs}_{GS}(hkl) \quad \text{(S14)}$$

$$\Delta\rho(\boldsymbol{r}) = \frac{1}{V}\sum_{hkl}^{n}[\left|F^{obs}_{ES}(\boldsymbol{H})\right| - \left|F^{obs}_{GS}(\boldsymbol{H})\right|]e^{i\varphi^{calc}_{GS}}e^{-i2\pi\boldsymbol{H}.\boldsymbol{r}} \quad \text{(S15)}$$

Where F^{obs} are the observed structure factors obtained from the GS and ES data sets, and one uses the phases from the GS model, for each measured reflection at reciprocal vector ***H***.

S2.2 Photoexcitation and Refinement details:

To obtain MS1 data set in CW case, the GS single crystal was irradiated with a CW laser of 422 nm (*P* = 120 mW) for 90 min at 100 K. For the transfer of MS1 to MS2 an LED of 940 nm (P = 200 mW) for 60 min was used. In molecule two, Ru2—N6—O2, no refinable MS2 was found as reported earlier [40]. For the generation of MS1, pulsed laser **A** (see Table 1 of main text for detail) (5 ns pulsed width, *f* = 10 Hz) at the wavelength 422 nm with *P* = 2.5 mW for 60 min, 280 min and 570 min was used. The corresponding data sets at three different time points were collected named as, MS1A after 60 min, MS1B after 280 min and MS1C after 570 min in order to follow the gradual evaluation of MS1 structural changes until photo stationary state of MS1 was reached. For the transfer of MS1 to MS2, pulsed laser **A** (see Table 1 in main text) (5 ns, *f* = 10 Hz) at the wavelength 940 nm with *P* = 2 mW for 120 min was used. After pulsed irradiation, compared to CW, significant population of MS2 was found in both the nitrosyls of molecule one and two.

The structures of complex **I** were solved in *P*-1 space group using the program *SHELXT* [31] and refined with least square method using *SHELXL* [32] embedded in *Olex2-1.5-alpha* suite [33]. Multi-scan absorption correction was performed using *LANA* embedded in *X-AREA* suite [30] and applied to all data sets. All the non-H atoms were refined anisotropically, except of the MS1B structure collected after pulsed irradiation, where both MS1 and GS components of the NO ligands were refined isotropically. In the refinement of all data sets, one or two of the perchlorate anions were disordered and were treated accordingly using EADP constraints in case of one particular perchlorate anion. It is to be noted that for the purpose of comparison the rest of the refinements of all data sets were performed at $(\sin\theta/\lambda)_{max}$ of 0.735 Å^{-1}. The corresponding data collection and refinement parameters are given in Table 2. The GS configuration of the nitrosyl groups for molecule one and molecule two was assigned as Ru1—N1—O1 and Ru2—N6—O2 while the MS1/MS2 configuration was assigned as Ru1—N1B—O1B and Ru2—N6B—O2B, respectively. In all structures after light irradiation the GS component bond distances of Ru1—N1 and Ru2—N6 were restrained to those of the pure GS Ru—NO

bond distances (1.768 and 1.760 Å, respectively) using DFIX restrain with 0.002 restrain constant. The bond distances of both GS nitrosyls N1—O1 and N6—O2 were restrained in a similar manner (to 1.153 and 1.149 Å, respectively) using DFIX with 0.002 restrain parameter. The atomic displacement parameters (ADP's) of nitrosyl groups in GS and MS1 were refined anisotropically and constrained using EADP constraint (only in case of MS1B structure the atoms of NO were refined isotropically to avoid non-positive defined ADP's). In all MS1 containing structures EADP constraints were applied as follows: ADP's of terminal atoms of nitrosyl ligands (O in case of GS and N in case of MS1) and coordinated atoms of NO (N in case of GS and O in case of MS1) were constraint by EADP separately, e.g. $U_{eq}(O_{GS}) = U_{eq}(N_{MS1})$ and $U_{eq}(N_{GS}) = U_{eq}(O_{MS1})$. MS2 structure obtained upon CW irradiation was refined without EADP constraint, whereas MS2 structure obtained upon pulsed laser irradiation was refined using EADP constraint on MS2 component on nitrosyl ligand: $U_{eq}(O_{MS2}) = U_{eq}(N_{MS2})$ to avoid non-positive defined ADP's.

Table S1: Uij's ($Å^2 \times 10^3$) of the selective atoms after CW and pulsed laser irradiation (U_{eq} is anisotropic thermal ellipsoids)

ADP [$Å^2 \times 10^3$]	*GS*	*MS1$_{CW}$*	*MS1$_{Pulsed}$*	*MS2$_{CW}$*	*MS2$_{Pulsed}$*
U_{eq} Ru1, Ru2	11.15(2), 11.09(2)	14.14(4), 14.05(4)	13.84(4), 13.68(4)	13.28(2), 12.62(2)	16.39(5), 16.82(5)
U_{eq} N1, N1B	14.3(2)	16.4(8), 26(1)	14.4(7), 27.4(9)	16.1(4), 22(2)	14.1(9), 64(9)
U_{eq} O1, O1B	22.6(2)	26(1), 16.4(8)	27.4(9), 14.4(7)	25.8(4), 18(2)	25.5(9), 64(11)
U_{eq} N6, N6B	13.9(2)	14.7(7), 23.8(8)	14.4(8), 23.3(9)	15.5(2)	18.5(8), 32(5)
U_{eq} O2, O2B	21.5(2)	23(8), 14.7(7)	23.3(9), 14.4(8)	24.3(2)	30.5(8), 32(5)

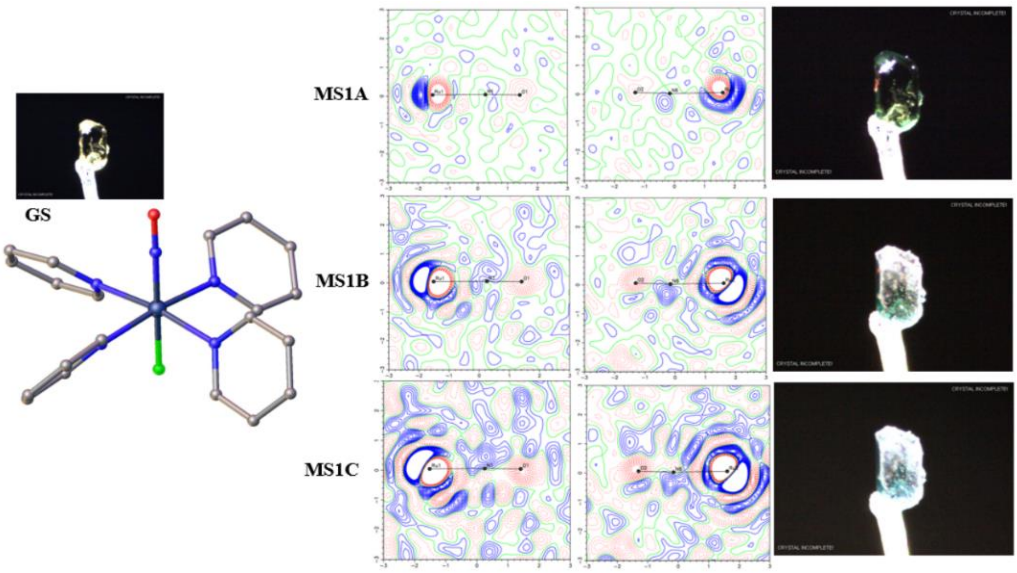

Figure S4: Photodifference maps of stepwise MS1 generation until saturation to about 85 % population in $[Ru(Py)_4(NO)F](ClO_4)_2$. The contours level for maps is 0.4 $eÅ^{-3}$.

Table S2: Crystallographic parameters of structures obtained during stepwise MS1 generation and its transfer to MS2 in $[Ru(Py)_4(NO)F](ClO_4)_2$.

$[Ru(Py)_4(NO)F](ClO_4)_2$	*GS*	*MS1A*	*MS1B*	*MS1C (PS1$_{Pulsed}$)*	*MS2 (MS2$_{Pulsed}$)*
Crystal data					
Chemical formula	$[Ru(NC_5H_5)_4(NO)F](ClO_4)_2$				
Crystal system, space group	Triclinic, *P*-1				
Temperature (K)	100(1)				
a, *b*, *c* (Å)	10.4675(16), 16.445(3), 16.580(6)	10.4966(11), 16.5384(15), 16.4489(16)	10.4708(13), 16.5282(15), 16.4320 (16)	10.5583(10), 16.4988(15), 16.3871(15)	10.4832(11), 16.4774(15), 16.5948(15)
α, β, γ (°)	66.97(2), 87.13(2), 83.187(14)	65.806(7), 86.968(8), 82.699(8)	65.753(7), 87.155(9), 82.621(9)	65.494(7), 87.581(8), 82.504(7)	65.819(7), 82.857(8), 87.089(8)
V (Å^3)	2602.2(12)	2583.5(5)	2571.4(5)	2575.0(4)	2594.7(5)
Z	4				
Radiation type	Mo *K*α				
μ (mm^{-1})	0.88				
Crystal size (mm^2)	0.1×0.2×0.28	0.2×0.2×0.4	0.2×0.2×0.4	0.2×0.2×0.4	0.2×0.2×0.4
Data collection					
Diffractometer	STOE STADI-VARI equipped with RebirX 540S CEGITEK Hybrid Pixel Area Detector (HPAD)				
No. of measured, independent and observed [$I > 2\sigma(I)$] reflections	55128, 22450, 18963	44443, 18968, 14587	45092, 19143, 15298	45052, 19050, 14803	46107, 19168, 14080
R_{int}	0.0144	0.0338	0.0364	0.0312	0.0311
Refinement					
$R[F^2 > 2\sigma(F^2)]$, $wR(F^2)$, *S*	0.0267, 0.0633, 1.112	0.0338, 0.0755, 1.056	0.0459, 0.0907, 1.102	0.0362, 0.0796, 1.087	0.0404, 0.0934, 1.086
No. of parameters	683	727	747	764	715
$\Delta\rho_{max}$, $\Delta\rho_{min}$ (e Å^{-3})	1.10, -0.93	1.10, -1.26	1.11, -2.25	1.45, -1.70	1.13, -1.59

Table S3: Selected crystallographic parameters of structures obtained during stepwise MS1 generation and its transfer to MS2 in $[Ru(Py)_4(NO)F](ClO_4)_2$. The atomic distance in Å and *U*ij's U_{iso}*/U_{eq}) in Å^2×10^3.

Bond length [Å]/ Angle [°]	*GS*	*MS1A*	*MS1B*	*MS1C (PS1$_{Pulsed}$)*	*MS2 (MS2$_{Pulsed}$)*
Ru1—N1	1.768(1)	-	-	-	-
Ru1—O1B	-	1.83(1)	1.845(4)	1.865(3)	2.19(3)

Ru2—N6	1.760(1)	-	-	-	-
Ru2 – O2B	-	1.83(2)	1.833(4)	1.855(3)	2.11(2)
Ru1—F1	1.933(1)	1.919(1)	1.905(2)	1.908(1)	1.921(2)
Ru2—F2	1.927(1)	1.920(1)	1.904(2)	1.904(1)	1.917(2)
N1—O1	1.153(1)	-	-	-	-
N1B—O1B	-	1.20(2)	1.144(5)	1.169(5)	0.97(3)
N6—O2	1.149(1)	-	-	-	-
N6B—O2B	-	1.14(4)	1.153(6)	1.155(4)	1.06(3)
Ru1—N1—O1	179.0(1)	-	-	-	-
Ru1—O1B—N1B O1B—Ru1—N1B	- -	162(3) -	177.7(4) -	177.2(8) -	64(3) 26(1)
Ru2—N6—O2	177.3(1)	-	-	-	-
Ru2—O2B—N6B O2B—Ru2—N6B	- -	169(10) -	169.9(9) -	175.7(7) -	70(2) 30(1)
U_{eq} Ru1, Ru2	11.15(2), 11.09(2)	11.37(4), 11.37(4)	13.49(5), 13.75(5)	13.84(4), 13.68(4)	16.39(5), 16.82(5)
U_{eq} N1, N1B	14.3(2)	12(1), 20(1)	13.9(6)*, 18(1)*	14.4(7), 27.4(9)	14.1(9), 64(9)
U_{eq} O1, O1B	22.6(2)	20(1), 12(1)	18(1)*, 13.9(6)*	27.4(9), 14.4(7)	25.5(9), 64(11)
U_{eq} N6, N6B	13.9(2)	13.6(6), 20.2(8)	14.3(6)*, 19.5(7)*	14.4(8), 23.3(9)	18.5(8), 32(5)
U_{eq} O2, O2B	21.5(2)	20.2(8), 13.6(6)	19.5(7)*, 14.3(6)*	23.3(9), 14.4(8)	30.5(8), 32(5)
Population [%]					
PLI(Mol. 1) GS(Mol. 1) PLI(Mol. 2) GS(Mol. 2)		26(2) 74(2) 15(2) 85(2)	69(2) 31(2) 60(3) 40(3)	85(2) 15(2) 87(2) 13(2)	19(1) 81(1) 14(1) 86(1)

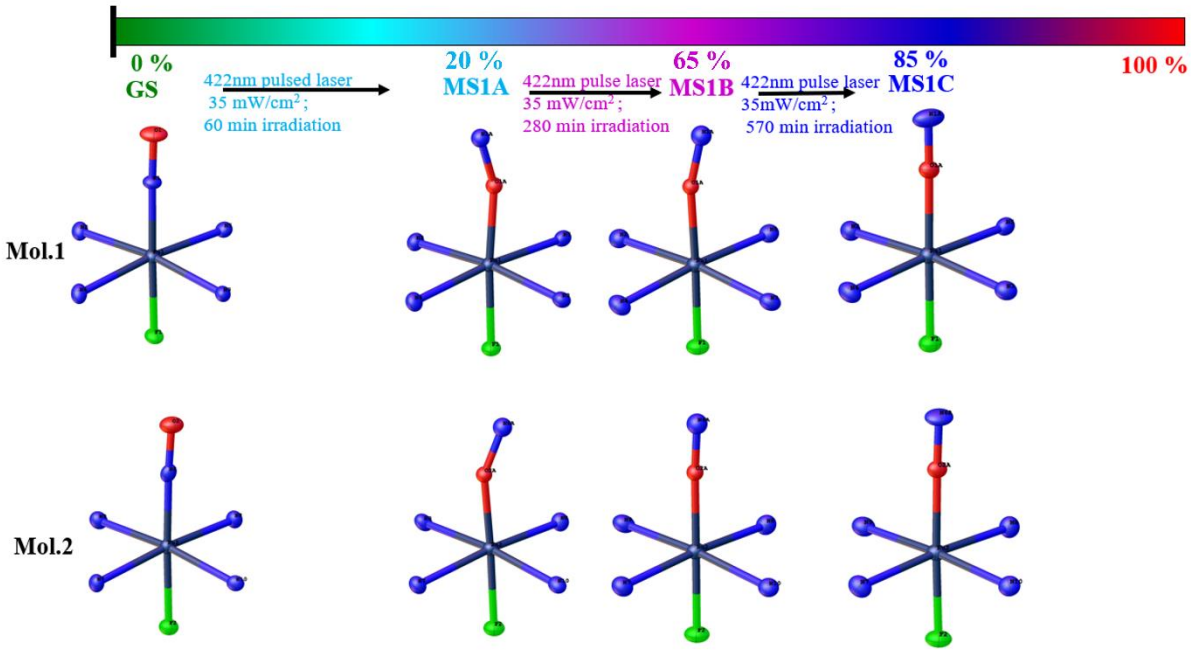

Figure S5: Systematic MS1 generation steps until saturation to about 85 % population in $[Ru(Py)_4(NO)F](ClO_4)_2$.

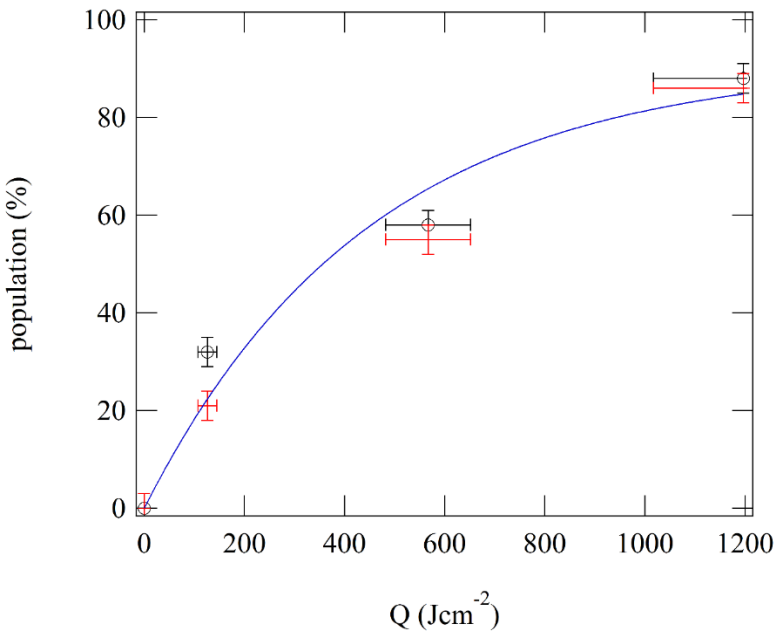

Figure S6: The population of MS1 as a function of Q. The line is a fit $P(Q) = P_{max}(1\text{-}\exp(-Q/Q_0)$ with $Q_0 =$ 450(200) J/cm^2 and $P_{max} = 91(16)$ %.